Monthly Notices
of the
ROYAL ASTRONOMICAL SOCIETY

MNRAS **462,** S242–S252 (2016)
Advance Access publication 2016 October 23

doi:10.1093/mnras/stw2720

The Agilkia boulders/pebbles size–frequency distributions: OSIRIS and ROLIS joint observations of 67P surface

M. Pajola,[1,2★] S. Mottola,[3★] M. Hamm,[3] M. Fulle,[4] B. Davidsson,[5] C. Güttler,[6] H. Sierks,[6] G. Naletto,[2,7,8] G. Arnold,[3] H.-G. Grothues,[9] R. Jaumann,[3,10] H. Michaelis,[3] J. P. Bibring,[11] C. Barbieri,[2,12] P. L. Lamy,[13] R. Rodrigo,[14,15] D. Koschny,[16] H. Rickman,[17,18] H. U. Keller,[19] J. Agarwal,[6] M. F. A'Hearn,[20] M. A. Barucci,[21,22] J. L. Bertaux,[23] I. Bertini,[2] S. Boudreault,[6] G. Cremonese,[24] V. Da Deppo,[8] S. Debei,[25] M. De Cecco,[26] J. Deller,[6] M. R. El Maarry,[27] C. Feller,[21] S. Fornasier,[21,22] A. Gicquel,[6] O. Groussin,[13] P. J. Gutierrez,[28] M. Hofmann,[6] S. F. Hviid,[3] W. H. Ip,[29] L. Jorda,[13] J. Knollenberg,[3] J. R. Kramm,[6] E. Kührt,[3] M. Küppers,[30] F. La Forgia,[12] L. M. Lara,[28] Z. Y. Lin,[29] M. Lazzarin,[12] J. J. Lopez Moreno,[28] A. Lucchetti,[24] F. Marzari,[12] M. Massironi,[31] H. Michalik,[32] N. Oklay,[6] A. Pommerol,[27] F. Preusker,[3] F. Scholten,[3] N. Thomas,[27] C. Tubiana[6] and J. B. Vincent[6]

Affiliations are listed at the end of the paper

Accepted 2016 October 19. Received 2016 October 18; in original form 2016 July 11

ABSTRACT

By using the images acquired by the OSIRIS (Optical, Spectroscopic and Infrared Remote Imaging System) and ROLIS (ROsetta Lander Imaging System) cameras, we derive the size–frequency distribution (SFD) of cometary pebbles and boulders covering the size range 0.05–30.0 m on the Agilkia landing site. The global SFD measured on OSIRIS images, reflects the different properties of the multiple morphological units present on Agilkia, combined with selection effects related to lifting, transport and redeposition. Contrarily, the different ROLIS SFD derived on the smooth and rough units may be related to their different regolith thickness present on Agilkia. In the thicker, smoother layer, ROLIS mainly measures the SFD of the airfall population which almost completely obliterates the signature of underlying boulders up to a size of the order of 1 m. This is well matched by the power-law index derived analysing coma particles identified by the grain analyser Grain Impact Analyser and Dust Accumulator. This result confirms the important blanketing dynamism of Agilkia. The steeper SFD observed in rough terrains from 0.4 to 2 m could point out intrinsic differences between northern and southern dust size distributions, or it may suggest that the underlying boulders 'peek through' the thinner airfall layer in the rough terrain, thereby producing the observed excess in the decimetre size range. Eventually, the OSIRIS SFD performed on the Philae landing unit may be due to water sublimation from a static population of boulders, affecting smaller boulders before the bigger ones, thus shallowing the original SFD.

Key words: methods: data analysis – methods: statistical – comets: individual: 67P C-G.

1 INTRODUCTION

On 2014 August 6, after a 10-year-long journey throughout the Solar system, the European Space Agency *Rosetta* spacecraft reached the Jupiter family comet 67P/Churyumov–Gerasimenko, hereafter 67P. Afterwards, the OSIRIS instrument (Optical, Spectroscopic and Infrared Remote Imaging System; Keller et al. 2007) onboard *Rosetta*,

★ E-mail: maurizio.pajola@nasa.gov, maurizio.pajola@gmail.com (MP); stefano.mottola@dlr.de (SM)

Table 1. The two OSIRIS NAC images and the ROLIS ones used for the presented analysis. The OSIRIS images were taken when *Rosetta* was at 3.4 au from the Sun, while the ROLIS ones were taken when *Rosetta* was at 3.0 au from the Sun.

Instrument	Date	UT	Distance (m)[(a)]	Scale (cm pixel^{-1})	Phase Angle(°)[(b)]	Field of View (m)
OSIRIS NAC	2014-09-14	17:31:24	28 160	53.0	63.9	1085.4
OSIRIS NAC	2014-09-14	17:47:55	28 150	53.0	63.9	1085.4
ROLIS	2014-11-12	15:32:59	67.4	7.1	33.9	72.5
ROLIS	2014-11-12	15:33:38	28.9	3.0	32.8	31.0
ROLIS	2014-11-12	15:33:58	9.0	0.95	32.3	9.7

[(a)]Spacecraft distance from the comet surface. [(b)]The phase angle in the ROLIS images varies by up to 50° from corner to corner. The phase angle listed in the table corresponds to the centre of the FOV.

got the most detailed high-resolution images of the comet, allowing an unprecedented characterization of its surface and activity.

The OSIRIS instrument is the scientific camera system onboard *Rosetta* (Keller et al. 2007). It is characterized by a Narrow Angle Camera (NAC) and a Wide Angle Camera (WAC) with a field of view (FOV) of 2.35° × 2.35° and 11.35° × 12.11°, respectively. Both cameras use a 2048 × 2048 pixel backside-illuminated CCD detector. The NAC has a spatial scale of 18.8 cm pixel^{-1} when it is at 10 km from the surface, while the WAC reaches a resolution of 1.01 m at the same distance. Both cameras present a set of filters, 11 for the NAC and 14 for the WAC, covering a wavelength range of 250–1000 nm and 240–720 nm, respectively.

A first, detailed description of OSIRIS early analysis on the nucleus structure, morphology and jets activity of 67P is available in Sierks et al. (2015) and in Thomas et al. (2015a). Despite its small dimensions, ∼4 km in diameter, 67P shows a wide morphological diversity: enveloping strata (Massironi et al. 2015), pits (Vincent et al. 2015), boulders (Pajola et al. 2015), high-reflectivity boulder clusters (Pommerol et al. 2015), local fracturing (El-Maarry et al. 2015), as well as dust covered terrains (Thomas et al. 2015b) are only some notable features which can be found on 67P.

After the *Rosetta* arrival, the so-called pre-landing phase started, focusing on an extremely detailed monitoring of 67P surface, lasting 2.5 months, and designed to allow the selection of the best landing site for the lander Philae. The high-resolution OSIRIS NAC images were used to produce the comet digital shape model (Preusker et al. 2015) fundamental to evaluate the slope constraints of the final landing site as well as the identification and measurements of boulders and production of hazard maps of the landing spot (Pajola et al. 2015). After a complex evaluation of five possible Philae landing sites summarized in Ulamec et al. (2015), the Agilkia one, located on the minor lobe of 67P and formerly known as J-site, was selected as the final landing site for Philae. On 2014 November 12, Philae was deployed from the *Rosetta* probe with a speed of 18.76 cm s^{-1}, when the spacecraft was at a distance of 22.5 km from the centre of the comet. Eventually, after 7 h of flight towards 67P, Philae made its historic touchdown on Agilkia (Bibring et al. 2015; La Forgia et al. 2015) bouncing on the surface and finally coming to rest on a different side of the small lobe of the comet, called Abydos (Lucchetti et al. 2016).

The lander descent towards 67P was documented by the ROsetta Lander Imaging System (ROLIS) – the descent and close-up camera onboard Philae (Mottola et al. 2007). ROLIS is a compact 1024×1024 pixel CCD imager mounted on the Philae instrument deck, with its viewing direction oriented nadir. In the descent configuration ROLIS has an FOV of 56.6° × 56.6° and observes in the clear spectral band. The first ROLIS images of the surface of the comet were obtained at a range of 3100 m with a corresponding scale of 3.3 m pixel^{-1}. Afterwards, the camera was set into a continuous, ring-buffer acquisition mode, with a frame rate of 0.1 Hz. The sequence was terminated by the touchdown signal, and the latest images, the ones with the highest spatial resolution, were relayed to the orbiter. This sequence resulted in the acquisition of seven images from a distance of 67 m down to 9 m from the surface, with a scale ranging between 7.1 and 0.95 cm pixel^{-1}, respectively (Mottola et al. 2015). Eventually, by comparing the images obtained by ROLIS and OSIRIS, the first Philae touchdown was confirmed well inside the predicted landing ellipse, at a distance of 130 m from its centre.

By using the images of both instruments, the analysis of the wide context of the Philae landing site is made possible, corroborated by the highest resolution images available of the Agilkia surface. Indeed, the simultaneous exploitation of this data set provides the nonpareil possibility to derive a complete size–frequency distribution (SFD) in the range between 0.05 and 30.0 m, i.e. to determine the structure of the cometary regolith spanning from pebbles (diameters ≤ 0.25 m) to boulders (diameters > 0.25 m).[1] The comparison between the results obtained from previous works on this topic (Pajola et al. 2015, 2016a; Pommerol et al. 2015; Vincent et al. 2016) provides fundamental hints to understand if similar boulder/pebble formation and degradation processes occur in such wide range of dimensions. Moreover, our studied size range overlaps the ones described in the 67P coma by Rotundi et al. (2015), Davidsson et al. (2015) and Fulle et al. (2016a); therefore, comparisons between our SFD analysis and the one inferred for coma particles can yield important information regarding the dust lifting processes occurring on the cometary surface.

The structure of this paper is here as follows. After the description of both the OSIRIS and ROLIS data sets and methods, we will focus on the results obtained on the surface of 67P. The resulting boulders/pebbles SFD will then be presented together with the implications on the properties of 67P cometary regolith. Moreover, a contextualization of the obtained results with previous studies performed on 67P will be presented too.

2 DATASET AND METHODS

Our multi-instrument analysis of the Agilkia surface is based on two OSIRIS NAC images taken on 2014 September 14, and on three of the seven ROLIS images taken during the Philae landing phase of 2014 November 12. The observation geometries, scales and phase

[1] Following the official USGS size terms after Wentworth (1922), 'boulders' have diameters >0.25 m, 'cobbles' range between 0.25 and 0.064 m, while 'pebbles' sizes range between 0.064 and 0.002 m. Since inside the Rosetta team the word 'cobbles' has never been used, while it has been used 'pebble' (Poulet et al. 2016; Blum et al. submitted), it could lead to misunderstandings. For this reason, we suggest here to use the word 'pebble' for the 0.25 m > size > 0.002 m range. Below 0.002 m the term 'particle' is used.

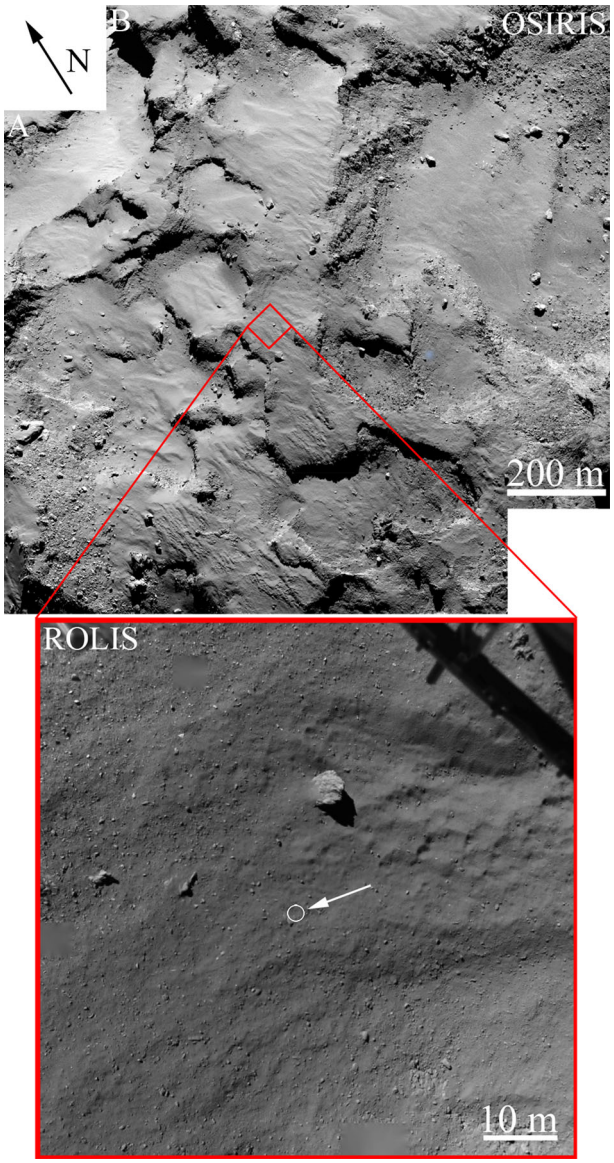

Figure 1. Upper panel: mosaic of the two OSIRIS NAC images taken on 2014 September 14, at 17.47.55 UT (A) and at 17.31.24 UT (B). Both images have a scale of 0.53 m pixel^{-1}. Lower panel: ROLIS image taken on 2014 November 12 at 15:32:59 UT at a distance of 67.4 m from the surface of the comet. The scale of this image is 7.1 cm pixel^{-1} and the FOV is 72.5 × 72.5 m^2. The white circle indicated with the arrow shows the location of the touchdown. The structure on the top right is part of the Philae landing gear. N arrow shows the direction of the north.

angles of the different data sets used in this paper are presented in Table 1. The OSIRIS images were taken at similar distances from 67P, i.e. 30.16 and 30.15 km from the comet centre, resulting in a scale of 53 cm pixel^{-1}. These images were taken during the pre-landing high-resolution OSIRIS observation campaign of the comet surface, in order to identify all surface features located on the Philae landing site and its surroundings, prior to the lander descent (Fig. 1, top panel). On the contrary, the ROLIS images were taken while Philae was approaching Agilkia, from an altitude ranging between 67 and 9 m far from the surface: their scale varies between 7.1 and 0.95 cm pixel^{-1}. The first image of the ROLIS data set is presented in the bottom panel of Fig. 1, while the entire area observed by ROLIS is enclosed in the red square presented in the OSIRIS context image of Fig. 1, top panel.

The multiresolution data set provided us with the unique opportunity to identify the location and the SFD of boulders/pebbles ranging between 0.05 and 30.0 m. On the OSIRIS images, we made use of the ARCGIS 10.1 software to manually identify the boulders present on the different types of terrains on the Agilkia landing site. Given the 53 cm pixel^{-1} scale of the images, we decided to stop at a 2.5 m minimum boulder size, i.e. the lowest statistically significant dimension, because below this value, the distribution starts to level off indicating incompleteness of the SFD (Mazrouei et al. 2014). Moreover, the 2.5 m limit value provides a meaningful and trustful size–frequency statistics, exceeding the three-pixel sampling rule (Nyquist 1928): this criterion guarantees the minimization of the features misidentifications. Since the observations were performed at a phase angle of ∼64°, elongated shadows on the surface provided the possibility of identifying even smaller boulders (3–4 pixels in diameter, ∼1.5–2.0 m). Nevertheless, we decided to exclude these smaller boulders for the sake of completeness. This approach is commonly used in boulders identification and analysis, as presented for example in Michikami et al. (2008), Mazrouei et al. (2014) and Pajola et al. (2015).

Following Pajola et al. (2016b,c), we defined a 'boulder' as a positive relief detectable, at least, in two images[2] obtained with different observation geometries, with the consistent presence of an elongated shadow (if the phase angle is greater than 0°). The identification was further facilitated by the fact that the boulder seems to be detached from the ground where it stands. Once these features were manually identified in the high-resolution images, we measured their position on the surface of the comet, assumed their shapes to be circumcircles and derived their maximum length, i.e. the diameter, and the corresponding area (see Fig. 2).

For evaluating the boulder/pebble sizes in the images acquired by ROLIS, a semi-automatic approach was chosen. The objects were first visually identified based on their shape, their appearance with respect to the background and the presence of a shadow. The outline of each boulder/pebble was then interactively approximated by a polygon. The resulting tagged area was used as a proxy for the projection of the boulders surface. The size of this area was automatically extracted from the images. The boulders linear metric size was then defined as the diameter of an equivalent sized circle. Quite obviously, a reliable identification of the pebbles becomes more difficult as the resolution limit is approached. Therefore, in order to avoid skewing the SFD, we only included pebbles in the counting which have a size of about four times the respective image pixel scale, similarly to what was done for the OSIRIS data set. Three ROLIS images acquired during the Philae descent were used for evaluating the SFD: the first, the fifth and the last image of the sequence. With this choice, we sampled the whole pebble/boulder size range covered by ROLIS, from about 5 cm to 5 m (see Fig. 3).

After identifying all possible boulders/pebbles in both the OSIRIS and ROLIS images, the obtained data were then binned with a constant bin size in logarithmic scale, such that the bin limits are $D_{i+1}=D_i\sqrt{2}$. By means of this representation, the incremental power-law slopes present the same index as the cumulative power law (Hartmann 1969). Then, in order to obtain the incremental

[2] We underline that the boulders which are not located on the overlapping area of Figs 1(A) and (B) were double checked on other OSIRIS NAC images not specifically centred on Agilkia. Consequently, they are not presented here.

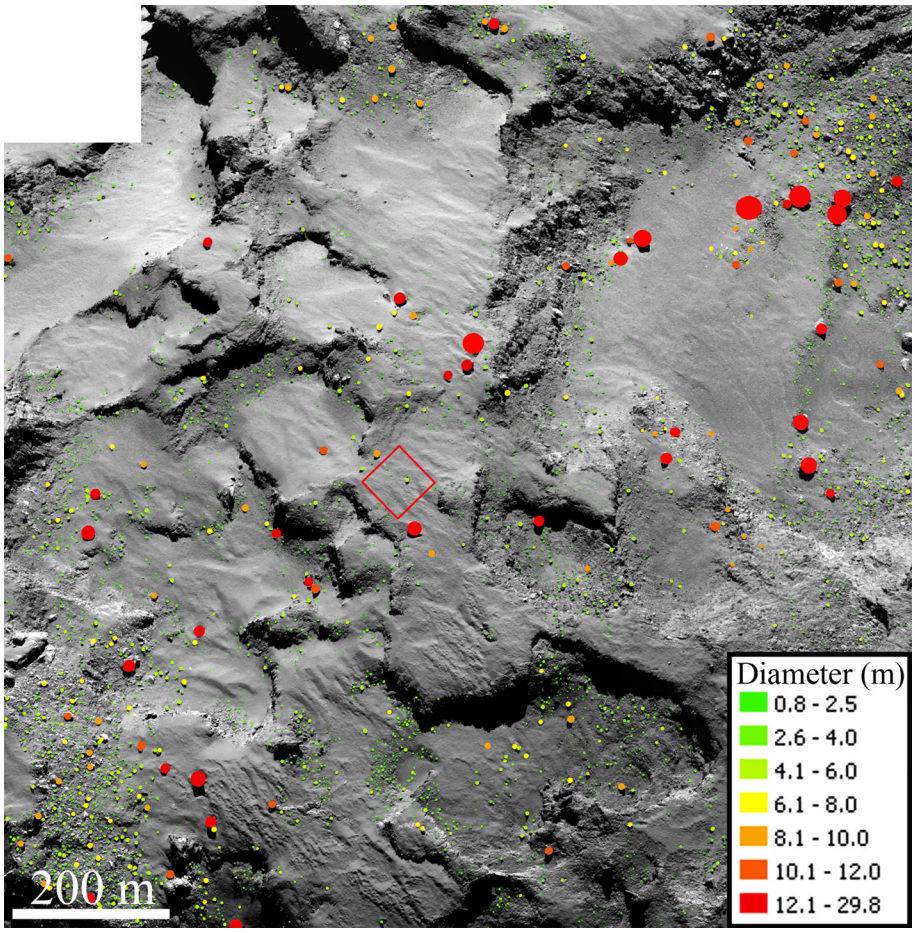

Figure 2. The spatial distribution of the boulders identified on the OSIRIS images on Agilkia. The boulders are classified on their different sizes. As for Fig. 1, the red square shows the ROLIS FOV of the first image acquired at 15.32.59 UT of 2014 November 12 and presented in Fig. 3(A).

boulder SFD per metre^2 for both the data sets, we measured the corresponding area extracted from the 3D shape model (SHAP5) of 67P (Preusker et al. 2015), Fig. 4.

Subsequently, in order to describe the gravitational framework of Agilkia, we computed the gravitational slope of the terrain pixel by pixel for the two OSIRIS context images (Fig. 5). The 3D model, decimated to 1.5×10^5 facets, has been used to derive the gravitational potential of this highly irregular comet, assuming an homogeneous nucleus with a density of 470 kg m^{-3} (Sierks et al. 2015) following the theory of Werner & Scheeres (1997) and accounting for the centrifugal force (Rossi & Fulchignoni 1999) due to the comet rotation (12.40 h, as from Mottola et al. 2014). The derived gravitational slope is then defined as the angle between the local surface normal pointing inside the nucleus and the gravity vector.

3 CURRENT KNOWLEDGE OF 67P BOULDER POWER-LAW INDICES

Before presenting the results we obtained on the OSIRIS and ROLIS data sets, and in order to help the reader throughout the following SFD results and discussion, we provide here the current context about the cometary boulder power-law indices. By making use of the first OSIRIS high-resolution images of 2014 August and September, Pajola et al. (2015) and Pajola et al. (2016b)[3] invoked several boulder formation processes which occurred and are still occurring on the changing surface of the comet. Indeed, by considering similar geomorphological settings on different locations of 67P, Pajola et al. (2015) suggested that each one of these different formation processes is characterized by its own specific SFD range. In the case of the formation of a pit after ceiling collapse, with a boulder field at its bottom, high boulder cumulative power-law indices ranging between −5.0 and −6.5 have been identified on 67P, indicative of high fragmentation resulting from a depression formation with subsequent escape of high-pressure volatiles. Once the pit is formed, thermal stresses and heat affect the exposed interior of the comet, thus intensifying fragmentation of the pre-fractured walls or formation of new fractures inside the mixture of dust and ices (Hoefner et al. submitted). This process results in sublimation both from the walls and from the newly formed boulders, which can be constituted of dust, ices or a mixture of both. As fracturing progresses, sustained sublimation occurs, the cliff is progressively eroded (Keller et al. 2015) and gravitational events occur, with the consequent formation of boulder fields at the foot of the cliffs.

[3] In fig. 8 of Pajola et al. (2016b), the schematic representation of the different types of boulder field formation, and the related power-slope ranges is depicted, while we provide here a brief summary of that.

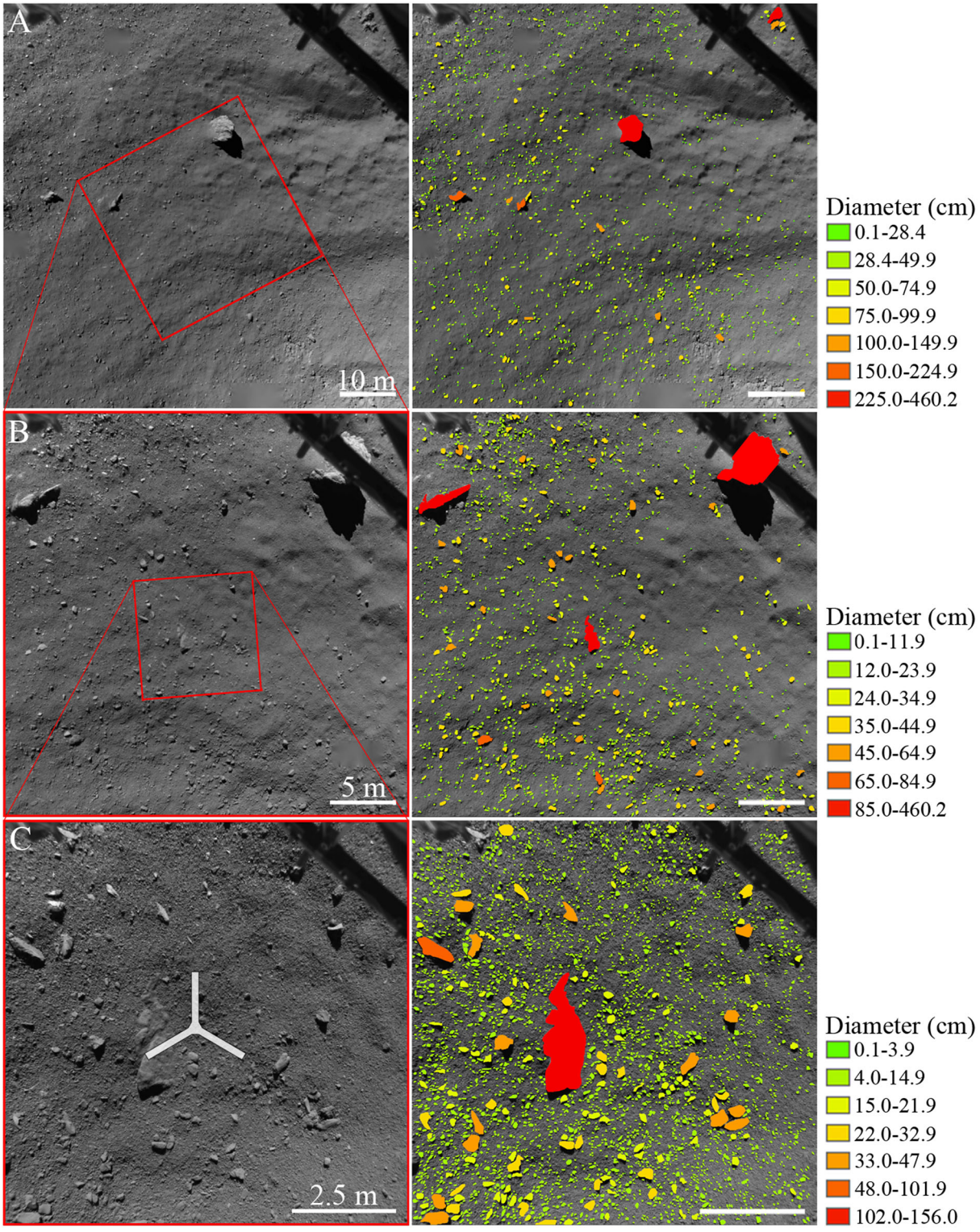

Figure 3. The spatial distribution of the boulders/pebbles identified on the three ROLIS images of Agilkia, see Table 1. The boulders/pebbles are classified on their different sizes. For completeness, in Fig. 3(C), we also added the final touchdown orientation of the three legs of Philae, as reconstructed by Biele et al. (2015).

Cumulative power-law indices ranging between −3.5 and −4.5 have been observed to be indicative of these phenomena. As the diameter of the pit increases, due to regressive erosion, the depression is continuously infilled with eroded material coming from the edges. Therefore, the boulder fields formed at the foot of the walls are continuously replenished by fresher material. On the contrary, the remnant boulders formed during the initial ceiling collapse may continue to sublimate and evolve, but they are progressively depleted, not being replenished by the retreating walls. This process, coupled with the degradation of the smaller boulders, is invoked to

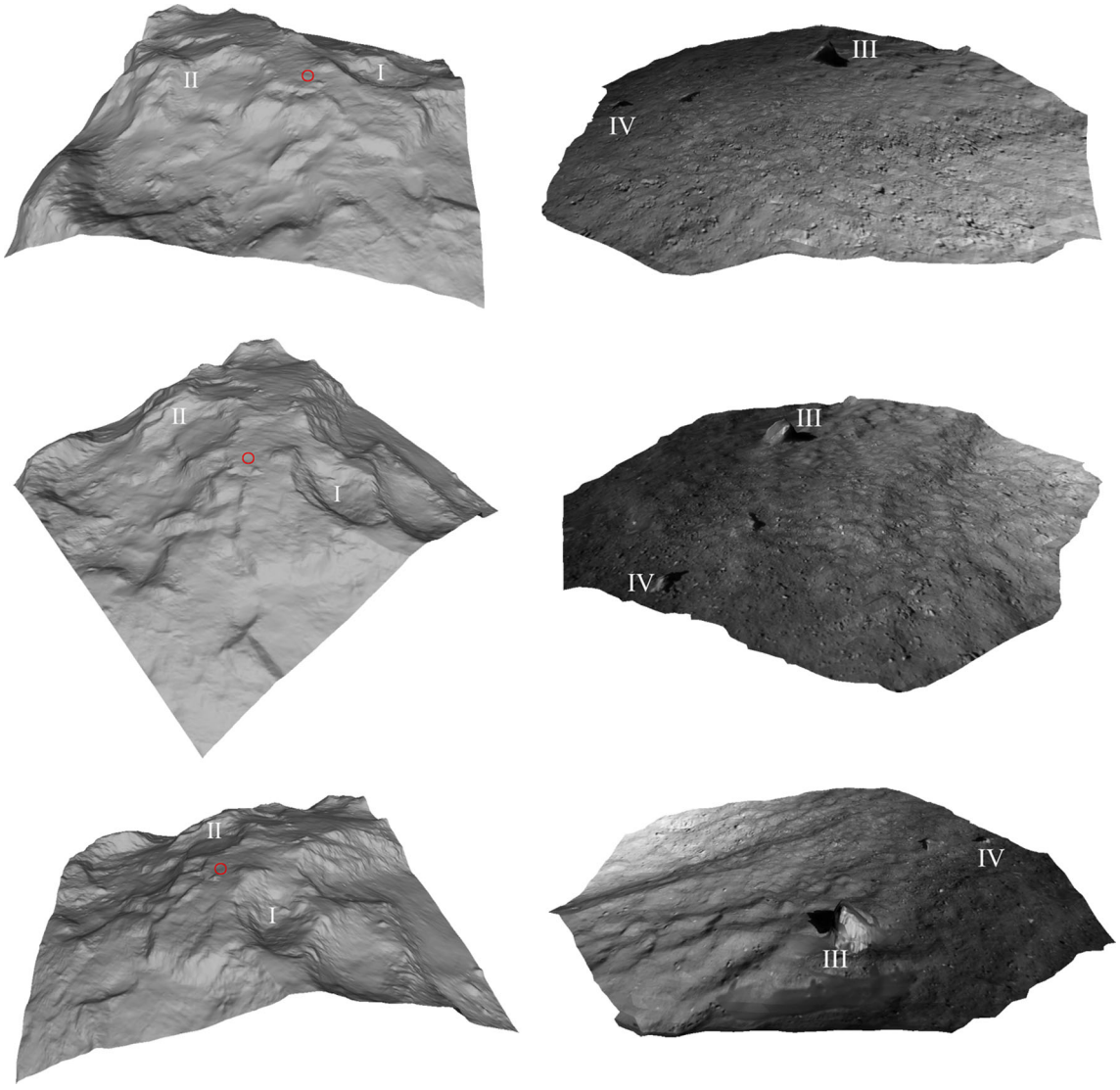

Figure 4. Left-hand panel: three different DTM views of the Agilkia site with a spatial resolution of 2 m. The red circle indicates the location of Philae's touchdown. I and II show the same two surface features on the site, and they are inserted in order to help the reader to understand the different geometry views. Right-hand panel: three different DTM views of the Agilkia site as observed by ROLIS camera. III and IV show the same two surface features on the area.

explain power-law indices below −3.0, and possibly from −1.0 to −2.0.

4 RESULTS

By means of the NAC context images, we have identified the boulders present on the different terrains of Agilkia. In total, we counted 3920 boulders, 2747 of which being ≥2.5 m. The area of Agilkia, based on the 3D shape model of 67P (Preusker et al. 2015), is 1.71 km^2. The spatial distribution of all the identified boulders is presented in Fig. 2. The largest boulders identified reach a maximum size ∼30 m, and they are located inside the Hatmehit depression (El-Maarry et al. 2015) ∼600 m east from the Philae touchdown location.

We consequently used the area extracted from the shape model of 67P, see Table 2, in order to get the incremental SFD per metre^2 of the context area. By fitting a regression line to the data, we derived a power-law index of −2.8 ±0.2, computed in the size range between 2.5 and 30 m (see Fig. 6). The frequency of boulders ≥2.5 m on the Agilkia context area is 1.8×10^{-3} m^{-2}.

We then focused on understanding what kind of power-law index is derivable from the OSIRIS boulder data set, but extracted only from the area which contains ROLIS measurements. In order to do so, we selected the morphologically homogenous area of Agilkia (La Forgia et al. 2015), which contained the field imaged by ROLIS during its descent. The gravitational slope map, coupled with the 3D shape model, helped us in defining the boundary of the yellow region presented in Fig. 7. This area is located on the fine material deposit on the layered terrain described in La Forgia et al. (2015); it is 0.20 km^2 wide and it hardly exceeds 10° slope (see Fig. 5). By fitting a regression line to the data, the power-law index we obtained from the incremental SFD per metre^2 of this area is −1.8 +0.2/−0.1, with a frequency of boulders ≥2.5 m of 0.5×10^{-3} m^{-2}.

From the boulder/pebble identification performed on the three ROLIS data set, we derived a total number of 1644 boulders/pebbles, 1481 ≥ 0.27 m have been identified in Fig. 3(A), 1784

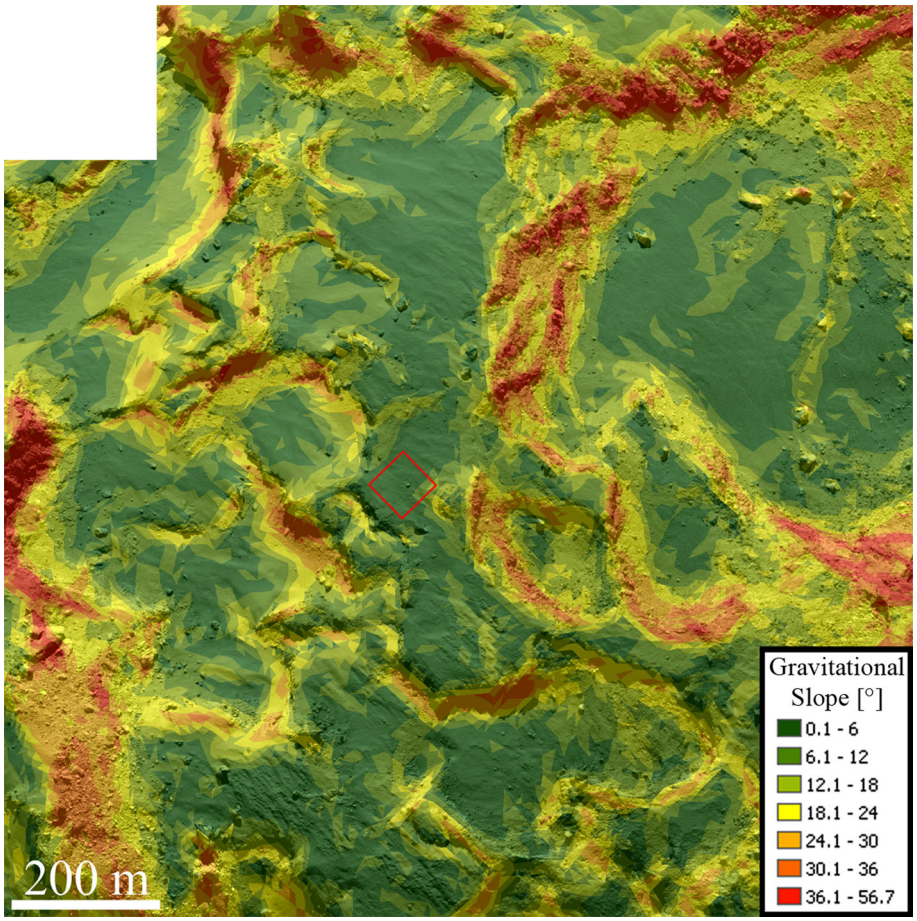

Figure 5. The gravitational slope maps produced with the observation geometry of the two OSIRIS NAC images. The values presented are in degree. The Philae landing site is identified with the red square. On this side of the small lobe of 67P, no gravitational slopes bigger than 60° are present. The steepest slopes are located on the rims of the Hatmehit depression (El-Maarry et al. 2015), i.e. east from the Philae landing spot, and on the Nut landslide, located west. A close inspection of the Philae area observed by ROLIS camera shows that there are very few slopes bigger than 6°, i.e. a particularly flat area.

Table 2. The 3D values of the areas used to compute the frequency of boulders/pebbles per metre^2 both on OSIRIS and ROLIS images.

Instrument	Fig. no.	Area (m^2)	Notes
OSIRIS	Fig. 2	1.7×10^6	Full image
OSIRIS	Fig. 7	0.2×10^6	Yellow area
ROLIS	Fig. 3(A)	4670.9	Full image
		3499.2	Left rough section
		1169.9	Right smooth section
ROLIS	Fig. 3(B)	864.4	Full image
		659.0	Left rough section
		205.8	Right smooth section
ROLIS	Fig. 3(C)	83.3	Full image
		55.2	Left rough section
		28.1	Right smooth section

boulders/pebbles, 1612 of which being ≥0.14 m in Fig. 3(B) and a total number of 2246 boulders/pebbles, 1812 ≥ 0.05 m have been identified in Fig. 3(C). The biggest boulder inside ROLIS data set is 4.6 m in diameter and it is located at a distance of ∼15 m from the Philae first landing location.

Despite the unprecedented resolution of the OSIRIS images, we were not able to distinguish different textures, and hence terrain types, inside the yellow area of Fig. 7. On the contrary, thanks to the higher resolution of the ROLIS data sets, it was possible to go

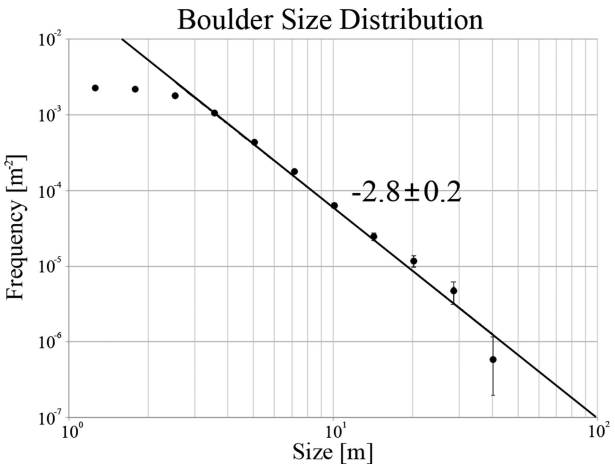

Figure 6. The incremental boulder/pebble SFD per metre^2 identified on the Agilkia context area of Fig. 2. The continuous lines represent a fitted regression line to the data. Vertical error bars indicate the root of the cumulative number of counting boulders, divided by the area computed from the 3D shape model of 67P. The power-law index of the size distribution is indicated too.

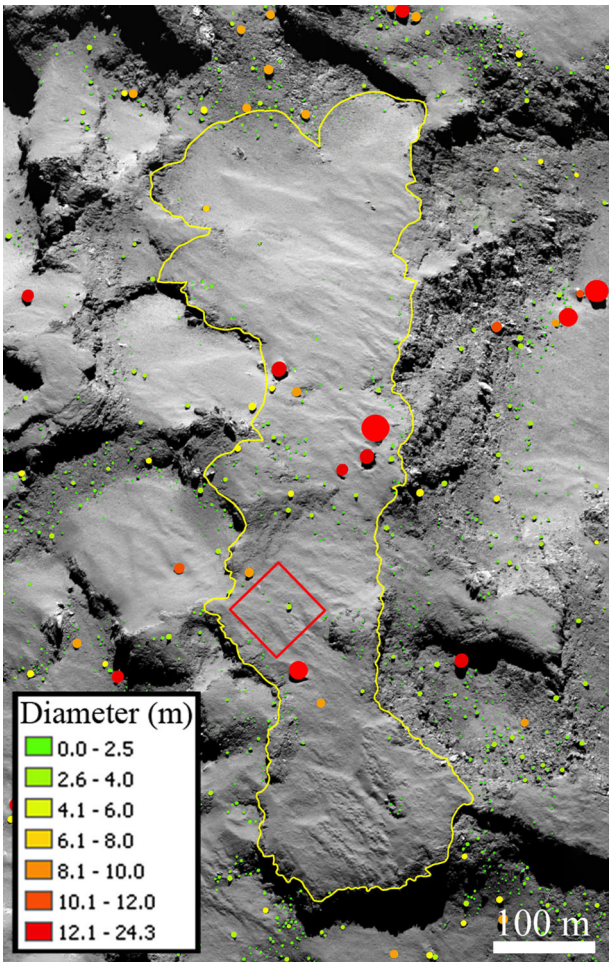

Figure 7. The spatial distribution of boulders identified on the OSIRIS NAC image on the geomorphological unit (yellow boundary) where Philae landed. As for Fig. 1, the red square shows the ROLIS FOV of the first image acquired at 15.32.59 UT of 2014 November 12, and presented in Fig. 3(A).

into much more detail on the surface, by distinguishing rough and smooth areas at the different scales (Fig. 8). From such distinction, three power-law indices have been derived by fitting the data. In the case of the rough terrain, two different power-slope indices were obtained, i.e. -2.2 ± 0.1, derived in the size range of 0.05–0.39 m, and -3.5 ± 0.3 from the size range of 0.39–2.19 m (Fig. 9). Conversely, on the smooth surface it was possible to derive a single power-law index of -2.8 ± 0.2, computed in the range spanning 0.05 and 1.1 m (Fig. 9). The frequency of pebbles $\geq$0.05 m ranges between 7.7 m^{-2} (smooth unit) and 12.3 m^{-2} (rough unit) while the frequency value of boulders $\geq$2.19 m is 0.6×10^{-3} m^{-2}.

5 DISCUSSION

5.1 Agilkia: global SFD case

The OSIRIS and ROLIS data sets complement each other. The first one provides a global view of the context area where Philae landed on 2014 November 12, the second one shows an extremely high-resolution zoom of Agilkia surface texture. Fig. 2 shows the diversity of terrains present on this part of 67P. As presented in La Forgia et al. (2015, fig. 5), five different types of terrain are located here, i.e. diamicton deposits, gravitational accumulation deposits, talus

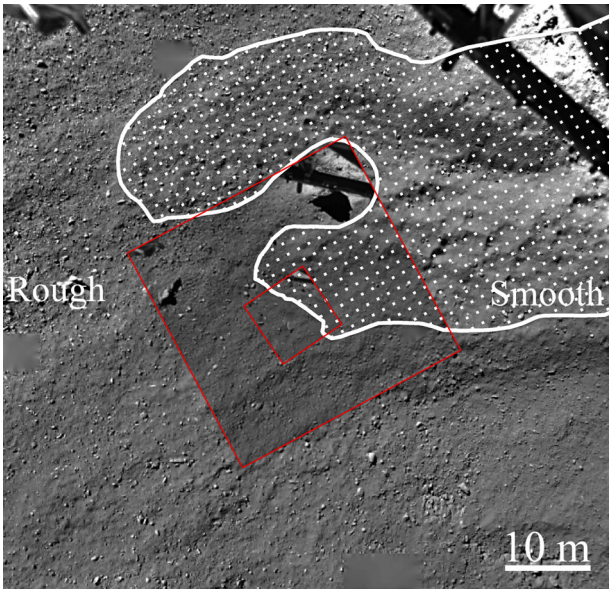

Figure 8. Mosaic of the three ROLIS images used in this paper. The distinction between the rough and the smooth units as observed by the descent camera is indicated with the white polyline.

deposits, fine material deposits located on the layered terrain and outcropping layered terrains. The global boulder size–frequency power-law index derived from the boulders of Fig. 2, and presented in Fig. 6, is -2.8 ± 0.2. This value does not fall inside any of the power-slope ranges presented in the context section. This is somehow expected, indeed we believe that this number may be indicative of properties of the source regions in combination with selection effects related to lifting, transport and redeposition. Yet, once localized and morphologically homogeneous areas inside this region are analysed, for example the Nut or the Hatmehit deposits (Pajola et al. 2015), the computed power-law indices return inside the expected mentioned ranges (-3.9 $+0.3/-0.2$ for the Nut deposit, -3.4 $+0.2/-0.1$ and -1.0 $+0.1/-0.2$ for the Hatmehit depression). Therefore, we suggest that steeper power-slope indices expected on taluses and pits, may be compensated by shallower power-law indices derived from the dusty, deeply processed deposits, returning the 'mixed' value which we measure.

5.2 Agilkia: local SFD case

In contrast, the localized measurements, performed on the yellow area of Fig. 7, are much more interesting and possibly representative of the processes which occurred/are still occurring on this area. In the case of OSIRIS localized measurements derived on the boulder statistics located inside the yellow area of Fig. 7, a power-law index of -1.8 $+0.2/-0.1$ was derived in the range 2.5–30.0 m. This is clearly shallower when compared to the indices derived by ROLIS; none the less, a comparable frequency in the range 2.0–3.0 m is present in both data sets, suggesting that both data set can be 'joined' together .[4] How is it possible to explain this difference in power-law SFD?

As modelled by Mottola et al. (2015) and Lai et al. (in press) and discussed in Keller et al. (2015) and Fulle et al. (2016b), the

[4] This can be seen in the black rectangle of Fig. 9, where a comparable frequency between OSIRIS Agilkia selection (0.5×10^{-3} m^{-2} at 2.5 m) and ROLIS data set (0.6×10^{-3} m^{-2} at 2.19 m) is observable.

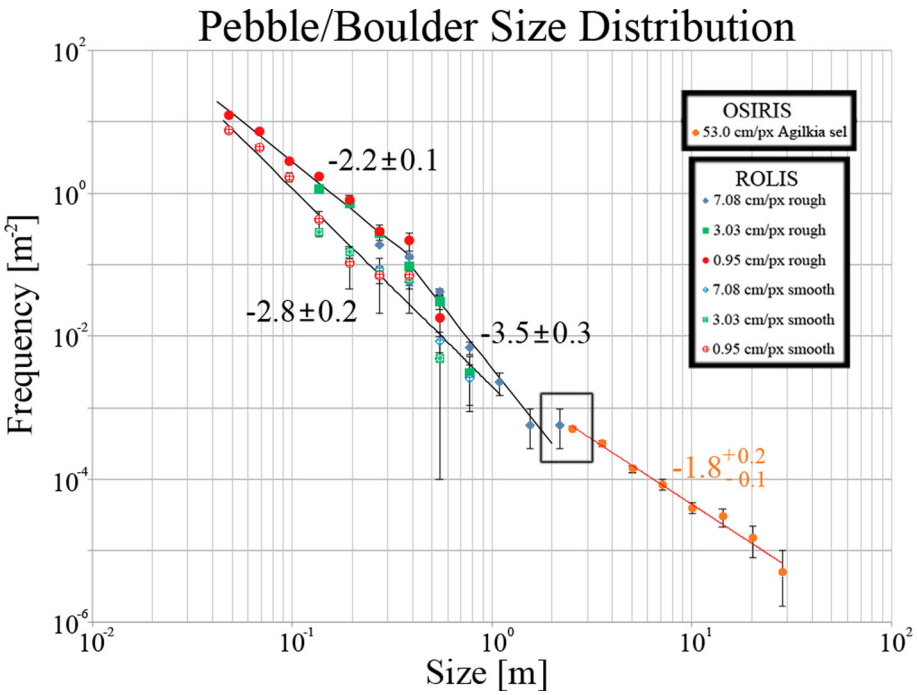

Figure 9. The pebble/boulder size–frequency incremental distribution per square meter identified on the Agilkia yellow area from OSIRIS (Fig. 7) and ROLIS (Fig. 3) data. The OSIRIS and ROLIS 3D areas used in this analysis are presented in Table 2. The continuous lines are fitted regression lines to the data. The power-law indexes of the size distributions are indicated too. The black rectangle shows the size range where the OSIRIS Agilkia selection and ROLIS data set 'join' together, having similar frequency values.

smooth terrains present on 67P are airfall deposits coming from south and occurring at perihelion on the northern hemi-nucleus, which is mostly in polar night during the short perihelion southern summer. The area of Agilkia is no exception, a clear dust blanket is present on its surface, suggesting that this side of the comet is characterized by an important seasonal dynamism (Lai et al. in press; Mottola et al. 2015).

The direct consequence of this blanketing process, is that the first Philae touchdown site might be partly or entirely mantled by a regolith layer consisting of airfall pebbles. This view is confirmed by the presence of a wind-tail and a 'moat' associated with a 5-m boulder in the ROLIS field. Via computer modelling, Mottola et al. (2015) have shown that these observed aeolian-like features are well explained by abrasion of a bedform by a nearly collimated flux of impinging pebbles. From a digital terrain model of the landing site, and from the identification of outcrops of what appears to be underlying bedrock, Mottola et al. (2015) estimate the thickness of this regolith layer to range from 0 to 50 cm for the rough terrain (see Fig. 8) and from 1 to 2 m in the smoother terrain. Therefore, it appears likely that the different SFD observed for the rough and smooth terrains may be due precisely to their different regolith thickness. Indeed, in the thicker, smoother layer, ROLIS would mainly measure the SFD of the airfall population, which would completely obliterate the signature of underlying boulders up to a size of the order of 1 m, while the underlying boulders could 'peek through' the thinner airfall layer in the rough terrain, thereby producing the observed excess in the decimetre size range.

In order to test such hypotheses, we have to consider the pebble SFD derived analysing the coma flying particles identified by Grain Impact Analyser and Dust Accumulator (GIADA) (Rotundi et al. 2015) and observed on OSIRIS images (Fulle et al. 2016b).

During the southern summer, the very low coma gas density on the nucleus night side is unable to affect the falling trajectories of dust larger than 1 mm (Fulle et al. 2016b); hence, the incremental size distribution of dust ejected at perihelion should match the one observed by ROLIS on the smooth plains. By analysing the data shown in fig. 6 of Fulle et al. (2016a), we obtained that a constant power law with incremental index of −2.7 is the best data fit over the entire observed mass range from 10^{-10} to 10^{2} kg. In the mass range from 1 to 100 kg, the observed size distribution is probably polluted by submetre-sized chunks in metastable orbits which are going to populate the chunk cloud orbiting 67P during the following aphelion (Rotundi et al. 2015). This explains the peak of the size distribution observed in these two upper mass bins. Moreover, we found that, assuming a constant power-law index of −2.7 from 1 to 100 kg, the dust-to-water mass ratio ranges from 10 to 15.[5] Fulle et al. (2016b) find that this water content in dust is consistent with the water loss rate from distributed sources in 67P coma, and therefore also with the water content in dust deposits explaining the activity observed from the northern hemi-nucleus during the following inbound comet orbit, when the northern hemi-nucleus is in summer (Keller et al. 2015; Fulle et al. 2016b). The power law with incremental index of −2.7 matches very well the ROLIS index of −2.8 observed in smooth plains (Fig. 9). The index of −2.8 also matches (within the index accuracy) the incremental index of −3 inferred during the inbound comet orbit (Rotundi et al. 2015; Fulle et al. 2016a) for the ejected dust of size larger[6] than 1 mm. By assuming that

[5] Taking into account that all the dust from 10^{-10} to 10^{2} kg has a water mass content of about 5 per cent, as discussed in Fulle et al. (2016b), the ratio between the dust loss rate and the water loss rate from the southern hemi-nucleus provides a dust-to-water mass ratio in the nucleus ranging from 10 to 15.

[6] Smaller ejected dust has a much shallower power index, close to −1 (Rotundi et al. 2015; Fulle et al. 2016a), and is out of ROLIS detection limits. This knee in the size distribution has been explained in terms of coma gas

dust deposits are characterized by the incremental index of −2.8, different index values are pointing out different dust and chunk populations. The steeper index of −3.5 observed by ROLIS in rough terrains from 0.4 to 2 m (Fig. 9) may point out intrinsic differences between northern and southern dust size distributions. A mixture of these two size distributions, the first shallower in the airfall deposits and the second steeper in the exposed northern hemi-nucleus, may explain the index −3 retrieved from coma observations during the inbound orbit (Rotundi et al. 2015; Fulle et al. 2016a), steeper than that observed in smooth plains (−2.8) and the one retrieved from coma observations at perihelion (−2.7). The much shallower index of −2.2 observed by ROLIS in rough terrains from 0.05 to 0.4 m may point out a selection effect occurring during the inbound orbit, when the gas density also at noon is too low to lift up dust larger than 0.4 m: the smaller the dust, the easier to eject these pebbles, the shallower the size distribution of pebbles remaining in rough terrains.

A similar effect cannot explain the even shallower index observed by OSIRIS from 2.5 to 30 m, since the considered sizes are much different with respect to those measured by ROLIS. A possible explanation that we invoke to explain this trend, may be water sublimation from a static population of boulders, which affects smaller boulders before the bigger ones, as proposed on other areas of 67P (Pajola et al. 2015, 2016b). Such effect would therefore decrease the frequencies of the smaller boulders identified on OSIRIS images, shallowing the original size distribution of boulders and possibly returning the power-law index we observe.

6 CONCLUSION

We made use of two OSIRIS NAC images taken on 2014 September 14, and on three of the seven ROLIS images taken during the Philae landing phase of 2014 September 12. Such multiresolution data set provided us with the unique opportunity to identify the location and the SFD of pebbles/boulders with sizes ranging 0.05–30.0 m on the Agilkia landing site.

This area of the comet, 1.7 km^2 wide, is characterized by five different types of terrain, i.e. diamicton deposits, gravitational accumulation deposits, talus deposits, fine material deposits located on the layered terrain and outcropping layered terrains. The global SFD measured on OSIRIS images over this area returns a power-law index of -2.8 ± 0.2, computed in the range 2.5–40.0 m. We suggest that this index reflects a mixture of the different properties of the multiple morphological units present on Agilkia, combined with selection effects related to lifting, transport and redeposition.

When the OSIRIS boulders, located on the morphologically homogeneous unit where Philae landed are analysed (fine material deposit located on the layered terrain), a much shallower SFD power-law index is derived: $-1.8\ {}^{+0.2}_{-0.1}$. This trend may be the result of water sublimation from a static population of boulders, affecting smaller boulders before the bigger ones, thus shallowing an originally steeper SFD. Contrarily, when the ROLIS much higher resolution images are studied, a smooth unit and a rough unit are identified with clearly distinct SFD. In the thicker, smoother layer, ROLIS mainly measures the SFD of the airfall population, -2.8 ± 0.2, which almost completely obliterate the signature of underlying boulders up to a size of the order of 1 m. This is well matched by the power-law index of −2.7 derived analysing coma particles identified by the GIADA instrument and observed on coma OSIRIS images. Indeed, during the southern summer, the very low coma gas density on the nucleus night side is unable to affect the falling trajectories of dust larger than 1 mm, and hence, the incremental size distribution of dust ejected at perihelion is expected to match the one observed by ROLIS on the smooth plains. This result confirms the important blanketing dynamism of Agilkia, supporting the interpretation that the smooth terrains present on 67P are airfall deposits coming from south. The steeper index of -3.5 ± 0.3 observed in rough terrains from 0.4 to 2 m could point out (i) an intrinsic difference between northern and southern dust size distributions which redeposit on Agilkia during different seasons, or (ii) it may suggest that the underlying boulders 'peek through' the thinner airfall layer in the rough terrain, thereby producing the observed excess in the decimetre size range. Eventually, the much shallower index of -2.2 ± 0.1 observed in ROLIS rough terrains from 0.05 to 0.4 m may point out a selection effect occurring during the inbound orbit, when the gas density also at noon is too low to lift up dust larger than 0.4 m: the smaller the dust, the easier to eject these pebbles, the shallower the size distribution of pebbles/boulders remaining in rough terrains.

density at perihelion in the northern polar night (Fulle et al. 2016a), which is too low to affect larger dust, but still strong enough to prevent the airfall of smaller dust, thus shallowing the airfall size distribution.

ACKNOWLEDGEMENTS

OSIRIS was built by a consortium of the Max-Planck-Institut für Sonnensystemforschung, in Göttingen, Germany, CISAS-University of Padova, Italy, the Laboratoire d'Astrophysique de Marseille, France, the Instituto de Astrofisica de Andalucia, CSIC, Granada, Spain, the Research and Scientific Support Department of the European Space Agency, Noordwijk, the Netherlands, the Instituto Nacional de Tecnica Aeroespacial, Madrid, Spain, the Universidad Politechnica de Madrid, Spain, the Department of Physics and Astronomy of Uppsala University, Sweden, and the Institut für Datentechnik und Kommunikationsnetze der Technischen Universität Braunschweig, Germany. The support of the national funding agencies of Germany (Deutsches Zentrum für Luft-und Raumfahrt), Italy (Agenzia Spaziale Italiana), France (Centre National d'Etudes Spatiales), Spain (Ministerio de Educación y Ciencia), Sweden (Swedish National Space Board) and the European Space Agency (ESA) Technical Directorate is gratefully acknowledged. We thank the ESA teams at European Space Astronomy Center, European Space Operation Center and European Space Research and Technology Center for their work in support of the *Rosetta* mission.

ROLIS was funded, built and managed by the DLR, German Aerospace Center, which we gratefully acknowledge. The ROLIS Team is indebted to the Lander Control Center (LCC, Cologne), CNES's Science, Operation, and Navigation Center (SONC) and the European Space Agency (ESA) for their support during the operations. We thank W. Bresch for his continued support during the development and operations of the experiment.

MP was supported for this research in part by an appointment to the National Aeronautics and Space Administration (NASA) Postdoctoral Program at the Ames Research Center administered by Universities Space Research Association (USRA) through a contract with NASA.

We made use of the ARCGIS 10.2 software together with IDL, MATLAB and R software to perform the presented analysis.

REFERENCES

Bibring J.-P. et al., 2015, Science, 349, aac5116
Biele J. et al., 2015, Science, 349
Blum J., Gundlach B., Johansen A., Agarwal J., Nature, in press

Davidsson B. J. R. et al., 2015, A&A, 583, A16
El-Maarry M. R. et al., 2015, A&A, 583, A26
Fulle M. et al., 2016a, ApJ, 821, 19
Fulle M., Altobelli N., Buratti B., Choukroun M., Fulchignoni M., Grün. E., Taylor M. G. G. T., Weissman P., 2016b, MNRAS, 462, S2
Hartmann W. K., 1969, Icarus, 10, 201
Hoefner S., Vincent J., Blum J., Davidsson B., Sierks H., El-Maarry M. R., Deller J., A&A, in press
Keller H. U. et al., 2007, Space Sci. Rev., 128, 433
Keller H. U. et al., 2015, A&A, 583, A34
La Forgia F. et al., 2015, A&A, 583, A41
Lai I.-L., Ip W.-H., Su C.-C., Lee J.-C., Lin Z.-Y., J.-S. W., Y. L., N. T., MNRAS, in press
Lucchetti A. et al., 2016, A&A, 585, L1
Massironi M. et al., 2015, Nature, 526, 402
Mazrouei S., Daly M. G., Barnouin O. S., Ernst C. M., DeSouza I., 2014, Icarus, 229, 181
Michikami T. et al., 2008, Earth Planets Space, 60, 13
Mottola S., Arnold G., Grothues H.-G., Jaumann R., Michaelis H., Neukum G., Bibring J.-P., 2007, Space Sci. Rev., 128, 241
Mottola S. et al., 2014, A&A, 569, L2
Mottola S. et al., 2015, Science, 349, 020232
Nyquist H., 1928, Trans. Am. Inst. Elect. Eng., 47, 617
Pajola M. et al., 2015, A&A, 583, A37
Pajola M. et al., 2016a, A&A, 585, A85
Pajola M. et al., 2016b, A&A, 592, A69
Pajola M. et al., 2016c, A&A, 592, L2
Pommerol A. et al., 2015, A&A, 583, A25
Poulet F. et al., 2016, MNRAS, 462, S23
Preusker F. et al., 2015, A&A, 583, A33
Rossi A., Fulchignoni M., 1999, Planet. Space Sci., 47, 873
Rotundi A. et al., 2015, Science, 347, aaa3905
Sierks H. et al., 2015, Science, 347, aaa1044
Thomas N. et al., 2015a, Science, 347, aaa0440
Thomas N. et al., 2015b, A&A, 583, A17
Ulamec S. et al., 2015, Acta Astronaut., 107, 79
Vincent J.-B. et al., 2015, Nature, 523, 63
Vincent J.-B. et al., 2016, A&A, 587, A14
Wentworth C. K., 1922, J. Geol., 30, 377
Werner R. A., Scheeres D. J., 1997, Celest. Mech. Dyn. Astron., 65, 313

[1]*NASA Ames Research Center, Moffett Field, CA 94035, USA*
[2]*Center of Studies and Activities for Space, CISAS, 'G. Colombo', University of Padova, Via Venezia 15, I-35131 Padova, Italy*
[3]*Deutsches Zentrum für Luft- und Raumfahrt (DLR), Institut für Planetenforschung, Rutherfordstrasse 2, D-12489 Berlin, Germany*
[4]*INAF Osservatorio Astronomico di Trieste, Via Tiepolo 11, I-34143 Trieste, Italy*
[5]*NASA Jet Propulsion Laboratory, 4800 Oak Grove Drive, Pasadena, CA 91109, USA*
[6]*Max-Planck-Institut für Sonnensystemforschung, Justus-von-Liebig-Weg 3, D-37077 Göttingen, Germany*
[7]*Department of Information Engineering, University of Padova, Via Gradenigo 6/B, I-35131 Padova, Italy*
[8]*CNR-IFN UOS Padova LUXOR, Via Trasea 7, I-35131 Padova, Italy*
[9]*Space Management, Space Science, DLR, Königswinterer Str. 522-524, D-53227 Bonn, Germany*
[10]*Institute of Geological Sciences, Freie Universität Berlin, D-12249 Berlin, Germany*
[11]*Institute of Space Astrophysics, F-91405 Orsay, France*
[12]*Department of Physics and Astronomy 'G. Galilei', University of Padova, Vic. Osservatorio 3, I-35122 Padova, Italy*
[13]*Aix Marseille Universite, CNRS LAM (Laboratoire d'Astrophysique de Marseille), UMR 7326, F-13388 Marseille, France*
[14]*Centro de Astrobiologa, CSIC-INTA, E-28850 Torrejon de Ardoz, Madrid, Spain*
[15]*International Space Science Institute, Hallerstrasse 6, D-3012 Bern, Switzerland*
[16]*Scientific Support Office, European Space Research and Technology Centre/ESA, Keplerlaan 1, Postbus 299, NL-2201 AZ Noordwijk ZH, the Netherlands*
[17]*Department of Physics and Astronomy, Uppsala University, SE-75120 Uppsala, Sweden*
[18]*PAS Space Reserch Center, Bartycka 18A, PL-00716 Warszawa, Poland*
[19]*Institute for Geophysics and Extraterrestrial Physics, TU Braunschweig, D-38106 Braunschweig, Germany*
[20]*Department for Astronomy, University of Maryland, College Park, MD 20742-2421, USA*
[21]*LESIA-Observatoire de Paris, CNRS, UPMC, Univ. Paris 06, Univ. Paris-Diderot, 5 Place J. Janssen, F-92195 Meudon Principal Cedex, France*
[22]*Univ Paris Diderot, Sorbonne Paris Cite, 4 Rue Elsa Morante, F-75205 Paris Cedex 13, France*
[23]*LATMOS, CNRS/UVSQ/IPSL, 11 Boulevard d'Alembert, F-78280 Guyancourt, France*
[24]*INAF Osservatorio Astronomico di Padova, Vic. Osservatorio 5, I-35122 Padova, Italy*
[25]*Department of Mechanical Engineering, University of Padova, Via Venezia 1, I-35131 Padova, Italy*
[26]*UNITN, University of Trento, Via Mesiano, 77, I-38100 Trento, Italy*
[27]*Physikalisches Institut der Universität Bern, Sidlerstr. 5, CH-3012 Bern, Switzerland*
[28]*Instituto de Astrofisica de Andalucia CSIC, Glorieta de la Astronomia, E-18008 Granada, Spain*
[29]*Institute for Space Science, National Central University, 32054 Chung-Li, Taiwan*
[30]*Operations Department, European Space Astronomy Centre/ESA, PO Box 78, E-28691 Villanueva de la Canada, Madrid, Spain*
[31]*Geosciences Department, University of Padova, Via G. Gradenigo 6, I-35131 Padova, Italy*
[32]*Institut für Datentechnik und Kommunikationsnetze der TU Braunschweig, Hans-Sommer-Str. 66, D-38106 Braunschweig, Germany*

This paper has been typeset from a TEX/LATEX file prepared by the author.